



## Characterization of bremsstrahlung and $\gamma$ -rays of fuel debris

Taichi Matsumura<sup>a,\*</sup>, Keisuke Okumura<sup>a</sup>, Manabu Fujita<sup>b</sup>, Masahiro Sakamoto<sup>a</sup>,  
Kenichi Terashima<sup>a</sup>, Eka Sapta Riyana<sup>a</sup>

<sup>a</sup> Japan Atomic Energy Agency, 790-1 Motooka Ohtsuka, Tomioka-machi, Futaba-gun, Fukushima-ken, 979-1151, Japan

<sup>b</sup> Japan Prime Computing Corporation, 851-12, Yokobori Naka-shi, Ibaraki-ken, 311-0103, Japan

### ARTICLE INFO

#### Keywords:

Fukushima Daiichi Nuclear Power Station  
Fuel debris  
 $\beta$ -ray  
Bremsstrahlung  
 $\gamma$ -ray  
Energy spectrum

### ABSTRACT

The characterization of bremsstrahlung and  $\gamma$ -rays from fuel debris differs from that of spent fuels evaluated to date, due to factors such as material composition and release of volatile fission products. In this work, in order to clarify the conditions under which the effect of bremsstrahlung compared to the total photons (bremsstrahlung and  $\gamma$ -rays) in fuel debris is maximized, the average energies and dose rates from the energy spectra of bremsstrahlung and  $\gamma$ -rays on the fuel debris surface were obtained using a Monte Carlo simulation. In the simulation, the average energies and dose rates were evaluated with consideration of the composition, size, fission product release, and retrieval time of the fuel debris. The simulation showed that the composition with the largest amount of change to the average total photons energy caused by bremsstrahlung was the molten fuel debris, and the composition with the maximum fraction of bremsstrahlung in the dose rate was the  $\text{UO}_2$ . The maximum value of the fraction of bremsstrahlung in the dose rate was evaluated to be about 17%. This work is expected to contribute to the prediction of the radiation characteristics of the fuel debris that will be retrieved from the Fukushima Daiichi Nuclear Power Station in the near future.

### 1. Introduction

The earthquake on March 11, 2011 that occurred on the Pacific coast of Tōhoku caused a tsunami that led to a loss-of-coolant accident (LOCA) at the Fukushima Daiichi Nuclear Power Station (1F). After the LOCA, melted fuel containing nuclear fuel ( $\text{UO}_2$ ), trans-uranium elements, and fission products (FPs) at high temperatures interacted with the cladding tubes (zircaloy), reactor pressure vessel (RPV) steels, and the concrete under the RPV and various types of fuel debris were formed. Based on the findings from the in-core situation assessment, internal investigations (IRID, 2020), and previous research (Terashima et al., 2021), we assumed three types of representative fuel debris in this study, they are un-melted  $\text{UO}_2$ , (U, Zr) $\text{O}_2$ , and Molten Core Concrete Interaction (MCCI) product.

In accordance with the roadmap (TEPCO, 2021) formulated by Tokyo Electric Power Company Holdings, Inc., it is planned to begin the retrieval of fuel debris from Unit 2, as a trial by the end of 2022, and to gradually increase the scale of the retrieval. In the initial phase, the size of the retrieved sample of fuel debris is expected to be a few centimeters. The radiation characteristics of the fuel debris are estimated to vary

depending on the composition and size. In addition, many conditions must be considered since the composition of the fuel debris changes over time due to the decay of radionuclides. Radionuclides in the fuel debris emit various types of radiation (OKUMURA et al., 2013a), but the dose (Terashima et al., 2021) and energy spectrum (Sapta RIYANA et al., 2020; Tomooki et al., 2017) of  $\gamma$ -rays, which have high dose rates and high permeability, have mainly been evaluated. Volatile FPs, such as Cs, are considered to be released during fuel melting, which differs from the radiation characteristics of  $\gamma$ -rays from conventional spent fuel. On the other hand, as  $\beta$ -rays decelerate in an object, they emit bremsstrahlung. The energy loss in this process is emitted as electromagnetic waves, i.e., photons. Like  $\gamma$ -rays, bremsstrahlung has high penetrating power and propagates its energy over long distances. In particular, the release of Cs from the fuel debris is expected to decrease the  $\gamma$ -rays, thus changing the relative fraction of bremsstrahlung and changing the average energy of the  $\gamma$ -rays and bremsstrahlung.

During  $\beta$ -decay, the energy of the decay is divided among the daughter nuclide, the electron, and the electron antineutrino, thus, the energy of the  $\beta$ -ray differs depending on the emission angle of the electron and the electron antineutrino. Therefore, the energy

\* Corresponding author.

E-mail addresses: [matsumura.taichi@jaea.go.jp](mailto:matsumura.taichi@jaea.go.jp) (T. Matsumura), [okumura.keisuke@jaea.go.jp](mailto:okumura.keisuke@jaea.go.jp) (K. Okumura), [fujita.manabu@j-pc.jp](mailto:fujita.manabu@j-pc.jp) (M. Fujita), [sakamoto.masahiro@jaea.go.jp](mailto:sakamoto.masahiro@jaea.go.jp) (M. Sakamoto), [terashima.kenichi@jaea.go.jp](mailto:terashima.kenichi@jaea.go.jp) (K. Terashima), [riyana.eka@jaea.go.jp](mailto:riyana.eka@jaea.go.jp) (E.S. Riyana).

<https://doi.org/10.1016/j.radphyschem.2022.110298>

Received 2 March 2022; Received in revised form 24 May 2022; Accepted 7 June 2022

Available online 16 June 2022

0969-806X/© 2022 Elsevier Ltd. All rights reserved.

distribution of  $\beta$ -rays shows a continuous distribution. When electrons pass near an atomic nucleus or another electron, they slow down due to the Coulomb force of the nucleus or electron, resulting in bremsstrahlung. The energy spectrum of bremsstrahlung produced by electrons is continuously distributed from the maximum energy of electrons incident on an object to zero, and the radiation yield increases as the atomic number,  $Z$ , of the atoms contained in the object increases (SELTZER et al., 1985). Since fuel debris contains high- $Z$  elements, such as uranium, it is assumed that bremsstrahlung will be generated with higher photon intensity and average energy than that emitted from contaminated water, which has been a problem in the past (Matsumura et al., 2020). Therefore, it is important to consider bremsstrahlung in the evaluation of fuel debris, unlike conventional spent fuel.

A fuel depletion calculation code ORIGEN has functions to consider bremsstrahlung in its photon source calculations (Bell, 1973). The general options for ORIGEN calculations are  $\text{UO}_2$  matrix (default option), water matrix, or no material. It has been indicated that the  $\text{UO}_2$  matrix option may be too conservative for  $\beta$ -rays present in low densities and low- $Z$  materials (Georgeta Radulescu et al., 2020). In addition, the spectra of  $\beta$ -rays emitted from various radionuclides in the fuel debris should be selected based on their maximum energy and intensity (radioactivity) in order to evaluate them reasonably from low to high energy. Thus the conventional fuel depletion calculation codes have not paid attentions to special situations like fuel debris.

The purpose of this study is to clarify the conditions under which the effect of bremsstrahlung is greatest by comparing the average energies and dose rates of bremsstrahlung and  $\gamma$ -rays on the fuel debris surface. For this purpose, we simulated the energy spectra and dose rates of bremsstrahlung and  $\gamma$ -rays at the fuel debris surface for different compositions, sizes, FPs release scenarios, and retrieval times using the theoretical equation for  $\beta$ -rays (KAI, 1955) and the Monte Carlo code of the Particle and Heavy Ion Transport code System (PHITS) (Sato et al., 2018). It was assumed that the radionuclides emitting  $\beta$ - and  $\gamma$ -rays were uniformly distributed in the fuel debris because localization of each radionuclide type was unknown.

## 2. Simulation method

### 2.1. Determining the simulation conditions

Mainly three conditions were employed to carry out the simulation. The creation of radiation sources to be used in the calculations is explained in Section 2.2. Specifically, Section 2.2 describes selection of the nuclides used as the  $\beta$ - and  $\gamma$ -ray sources, and production of  $\beta$ - and  $\gamma$ -rays from the selected nuclides. Section 2.3 describes the composition and geometry of the fuel debris modeled by simulation, and Section 2.4 describes the observed area of the energy spectra and dose rates of bremsstrahlung and  $\gamma$ -rays, along with the number of traced particles of the Monte Carlo methods.

### 2.2. Radiation sources

In order to evaluate the energy spectra and dose rates of the bremsstrahlung and  $\gamma$ -rays, it was necessary to produce  $\beta$ - and  $\gamma$ -rays from the fuel debris, which was the radiation source. The fuel debris at the time of the accident contained thousands of different radionuclides. In this study, we calculated bremsstrahlung and  $\gamma$ -rays emitted from the fuel debris using the decay data library JENDL/DDF-2015 (Jun-ichi KATAKURA et al., 2016) with the theoretical equation for  $\beta$ -rays [equation (1)] (KAI, 1955).

#### 2.2.1. Radioactivity of nuclides

The inventory data for the radionuclides contained in the fuel debris were determined based on publicly available data (NISHIHARA et al., 2012). Decay calculations based on the Chebyshev rational approximation method (CRAM) (Pusa, 2011) were performed on the inventory

data of Unit 2 immediately after the accident on March 11, 2011, and the secular changes of the inventory were taken into account. Two time points, 11 and 20 years after the accident (TEPCO, 2021), were selected for evaluation of the secular changes since samples and full-scale of fuel debris are scheduled to be retrieved at the both points in time. The decay calculations also accounted for the release of FP nuclides, which was based on the Phebus FPT4 (Bottomley et al., 2006), and two release rate patterns were considered in the decay calculations: zero release and volatile release of FPs. The assumed FPs release rates are shown in Table 1.

An inventory of four cases was assumed by combining the secular changes of inventory at 11 and 20 years after the accident and the FPs release rates. The four cases are shown in Table 2.

#### 2.2.2. Selection of nuclides

First, the  $\gamma$ -ray sources were created from 194  $\gamma$ -ray emitting nuclides using the inventory data described in Section 2.2.1 and JENDL/DDF-2015. Next,  $\beta$ -ray emitting nuclides were selected from the decay heat because, unlike  $\gamma$ -rays,  $\beta$ -rays cannot be directly generated from JENDL/DDF-2015. We considered the  $\beta$ -ray emitting nuclides in the ground state and excited states of each nuclide defined in JENDL/DDF-2015. The nuclides to be evaluated were selected to account for more than 99.9% of the total decay heat so that the effect on the final result to simulate the actual situation as closely as possible could be almost negligible. The nuclides contributing to the decay heat of  $\beta$ -rays for the Case 1, 2, 3, and 4 are shown in Table 3. The following 12 nuclides were selected:  $^{85}\text{Kr}$ ,  $^{90}\text{Sr}$ ,  $^{90}\text{Y}$  ( $^{90}\text{Sr}$ ),  $^{106}\text{Rh}$  ( $^{106}\text{Ru}$ ),  $^{125}\text{Sb}$ ,  $^{134}\text{Cs}$ ,  $^{137}\text{Cs}$ ,  $^{144}\text{Pr}$  ( $^{144}\text{Ce}$ ),  $^{147}\text{Pm}$ ,  $^{154}\text{Eu}$ ,  $^{155}\text{Eu}$ , and  $^{241}\text{Pu}$ . The nuclides shown in parentheses are the parent nuclides of short-lived nuclides in radiative equilibrium. For example,  $^{106}\text{Rh}$  with a half-life of 30.1 s is generated from the  $\beta$ -decay of  $^{106}\text{Ru}$  with a half-life of 1.02 years. The average  $\beta$ -ray energy of  $^{106}\text{Ru}$  is much lower than that of  $^{106}\text{Rh}$ . Although  $^{106m}\text{Rh}$  has a longer half-life (2.18 h) than  $^{106}\text{Rh}$ , it does not contribute to radioactivity of the fuel debris because it disappears shortly after the accident.

#### 2.2.3. Derivation of $\beta$ -rays for selected nuclides

Since  $\beta$ -decay nuclides have several branching ratios within the  $\beta$ -decay, they were combined to produce  $\beta$ -rays specific to each nuclide. The branching ratios, maximum energies, and spectral correction factors were obtained from the decay data of JENDL/DDF-2015. The  $\beta$ -ray of each nuclide was determined using the following theoretical equation (1) (KAI, 1955).

$$P(E_\beta)dE_\beta = k \cdot C(E_\beta) \cdot F(Z, W) \cdot p \cdot W \cdot (E_0 - E_\beta)^2 dE_\beta \quad (1)$$

where:

$W$  = Total energy of  $\beta$ -ray. ( $= E_\beta + m_e c^2$ )  $E_\beta$  = Kinetic energy of  $\beta$ -ray

**Table 1**  
Assumed FPs release ratios at the time of the accident.

Types	Elements	Release ratios	
		Release case <sup>a</sup>	Zero release case
Noble gas	He, Ne, Ar, Kr, Xe, and Rn	0.99	0.00
Volatile	I	0.97	0.00
FPs	Cs	0.84	0.00
	Te	0.80	0.00
	Mo	0.77	0.00
	Rb	0.53	0.00
	Cd	0.44	0.00
	Ba	0.35	0.00
	Sb	0.30	0.00
	Pd	0.27	0.00
	Ag	0.092	0.00
	Tc	0.071	0.00
	Ru	0.018	0.00
Sr	0.014	0.00	

<sup>a</sup> Based on Phebus FPT4 experiment (Bottomley et al., 2006).

**Table 2**  
The four cases defined by combining the elapsed time and the FPs release rates

Characteristics	Case conditions			
Case name	Case 1	Case 2	Case 3	Case 4
Elapsed time from 1F accident (years)	11 (TEPCO, 2021)		20 (TEPCO, 2021)	
FPs release scenarios	Zero release case	Release case based on Phebus FPT4 (Bottomley et al., 2006)	Zero release case	Release case based on Phebus FPT4 (Bottomley et al., 2006)

(MeV)

$P(E_\beta)dE_\beta$  = Probability that the  $\beta$ -ray is emitted with an energy between  $E_\beta$  and  $E_\beta + dE_\beta$   
 $E_\beta + dE_\beta$  = Momentum of emitted  $\beta$ -ray. (=  $(W^2 - 1)^{1/2}E_0$ )  
 $E_0$  = Maximum kinetic energy of  $\beta$ -rays emitted during  $\beta$ -decay.

$k$  = Constant.

$Z$  = Atomic number of the nucleus after decay.

$m_e$  = Rest mass of electron.

$c$  = Speed of light.

$F(Z, W)$  = Fermi function.

$C(E_\beta)$  = Spectral correction factor.

= 1: *allowed transition*.

=  $P^2 + (E_0 - E_\beta)^2$ : *First-forbidden transition*.

The Fermi function (2) is given by:

$$F(Z, W) = 2(1 + \gamma)(2pR)^{2(\gamma-1)} \exp(\pm\pi\gamma) \frac{[\Gamma(\gamma + iy)]^2}{[\Gamma(2\gamma + 1)]^2} \quad (2)$$

where:

$y = aZW/p$  ( $Z$ : Atomic number of the nucleus after decay)

$\gamma = [1 - (\alpha Z)^2]^{1/2}$   
 $\alpha = 2\pi e^2/hc$  ( $= 1/137$ )  
 $h$  = Planck's constant. (=  $6.62 \times 10^{-34} \text{ J}\cdot\text{s} = 6.62 \times 10^{-27} \text{ erg}\cdot\text{s}$ )  
 $e$  = Electrometric quantity. (=  $1.60 \times 10^{-19} \text{ C} = 4.80 \times 10^{-10} \text{ esu}$ )  
 $R = (1/2)\alpha A^{1/3} = 1.41 \times 10^{-13} A^{1/3} (\text{cm})$

**Table 3**  
The nuclides contributing to the decay heat of  $\beta$ -rays under the conditions of Case 1, 2, 3, and 4.

11 years after the accident				20 years after the accident			
Case 1: Zero FPs release case				Case 2: FPs release case based on Phebus FPT4 (Bottomley et al., 2006)			
Nuclides	Decay heat (W)	Fraction (%)	Cumulative Fraction (%)	Nuclides	Decay heat (W)	Fraction (%)	Cumulative Fraction (%)
<sup>90</sup> Y	2.19E+04	64.47	64.47	<sup>90</sup> Y	2.16E+04	77.56	77.56
<sup>137</sup> Cs	5.94E+03	17.49	81.95	<sup>90</sup> Sr	4.53E+03	16.26	93.82
<sup>90</sup> Sr	4.59E+03	13.51	95.46	<sup>137</sup> Cs	9.50E+02	3.41	97.23
<sup>85</sup> Kr	6.16E+02	1.81	97.28	<sup>147</sup> Pm	2.37E+02	0.85	98.08
<sup>147</sup> Pm	2.37E+02	0.70	97.98	<sup>154</sup> Eu	1.87E+02	0.67	98.76
<sup>154</sup> Eu	1.87E+02	0.55	98.53	<sup>241</sup> Pu	1.39E+02	0.50	99.26
<sup>134</sup> Cs	1.81E+02	0.53	99.06	<sup>106</sup> Rh	1.08E+02	0.39	99.65
<sup>241</sup> Pu	1.39E+02	0.41	99.47	<sup>134</sup> Cs	2.89E+01	0.10	99.75
<sup>106</sup> Rh	1.10E+02	0.32	99.80	<sup>144</sup> Pr	2.55E+01	0.09	99.84
<sup>144</sup> Pr	2.55E+01	0.07	99.87	<sup>155</sup> Eu	1.61E+01	0.06	99.90
<sup>125</sup> Sb	1.83E+01	0.05	99.92				
20 years after the accident				Case 4: FPs release case based on Phebus FPT4 (Bottomley et al., 2006)			
Case 3: Zero FPs release case				Nuclides	Decay heat (W)	Fraction (%)	Cumulative Fraction (%)
Nuclides	Decay heat (W)	Fraction (%)	Cumulative Fraction (%)	<sup>90</sup> Y	1.74E+04	78.95	78.95
<sup>90</sup> Y	1.76E+04	65.98	65.98	<sup>90</sup> Sr	3.64E+03	16.55	95.50
<sup>137</sup> Cs	4.83E+03	18.06	84.04	<sup>137</sup> Cs	7.72E+02	3.51	99.00
<sup>90</sup> Sr	3.70E+03	13.83	97.87	<sup>154</sup> Eu	9.07E+01	0.41	99.42
<sup>85</sup> Kr	3.45E+02	1.29	99.16	<sup>241</sup> Pu	9.00E+01	0.41	99.82
<sup>154</sup> Eu	9.07E+01	0.34	99.50	<sup>147</sup> Pm	2.20E+01	0.10	99.92
<sup>241</sup> Pu	9.00E+01	0.34	99.84				
<sup>147</sup> Pm	2.20E+01	0.08	99.92				

### 2.3. Materials and geometry

Although the specific nature of the fuel debris remains unknown, three typical types (IRID, 2020; Terashima et al., 2021) of fuel debris were assumed in this work: UO<sub>2</sub>, (U<sub>0.5</sub>, Zr<sub>0.5</sub>)O<sub>2</sub> (hereafter “molten debris”), and MCCI products. A sphere was assumed as the shape of the fuel debris for simplicity. The radius of the fuel debris was varied at 0.5 cm, 2.5 cm, and 5.0 cm. Table 4 shows other assumed characteristics of the fuel debris based on the literatures (IRID, 2020; Terashima et al., 2021; Bottomley et al., 2006; Olsen et al., 1988; OKUMURA et al., 2013b). The calculation conditions of the Monte Carlo simulation by PHITS are shown schematically in Fig. 1. The fuel debris was exposed to the air, and the  $\beta$ - and  $\gamma$ -rays were uniformly distributed in the fuel debris and emitted isotropically.

**Table 4**  
Characteristics of three types of fuel debris (IRID, 2020; Terashima et al., 2021; Bottomley et al., 2006; Olsen et al., 1988; OKUMURA et al., 2013b).

Characteristics	Types of Fuel debris		
Types of Fuel debris	UO <sub>2</sub>	Molten debris	MCCI products
Burnup in Unit 2 (Gwd/t)	23.1		
Elapsed time from 1F accident (years)	11, 20		
Radius $r$ (cm)	0.5, 2.5, 5.0		
True density $\rho$ (g/cm <sup>3</sup> )	10.96	8.00	4.05
Porosity (%)	0.00	21.50	33.50
Bulk density $\rho$ (g/cm <sup>3</sup> )	10.96	6.28	2.69
Uranium concentration $u$ (wt%)	88.15	57.92	7.88
Elemental composition	Concentration (wt%)		
Elements			
B	0.00	0.00	0.09
O	11.85	16.69	38.66
Na	0.00	0.00	0.99
Mg	0.00	0.00	3.26
Al	0.00	0.00	3.33
Si	0.00	0.00	19.40
K	0.00	0.00	3.54
Ca	0.00	0.00	4.76
Cr	0.00	0.00	0.85
Fe	0.00	0.00	13.61
Zr	0.00	25.39	3.45
La	0.00	0.00	0.16
Ce	0.00	0.00	0.04
U	88.15	57.92	7.88

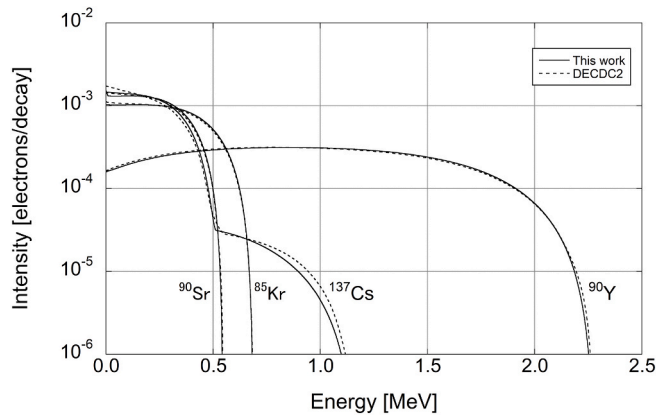


Fig. 1. Comparison of  $\beta$ -rays formed by typical  $\beta$ -ray emitting nuclides.

#### 2.4. Observation area (tally) and the number of traced particles

The observation area for bremsstrahlung and  $\gamma$ -rays emitted from the fuel debris was set on the air layer near the fuel debris surface. PHITS generates bremsstrahlung using the Bethe–Heitler cross-section (Sato et al., 2018). The T-Cross virtual detectors in the PHITS simulation were set in the observation region on the spherical shell to obtain the energy spectra and dose rates of bremsstrahlung and  $\gamma$ -rays. The dose rates were calculated using the photon flux and the conversion factor of the ambient dose equivalent  $H^*(10)$  (ICRP, 1996).

The number of traced photons in each PHITS simulation was  $1.0 \times 10^8$ . The value after “ $\pm$ ” in the following sections shows the statistical uncertainty ( $1\sigma$ ) of the Monte Carlo simulation by PHITS.

### 3. Results and discussions

#### 3.1. Comparison of the derived $\beta$ -rays

In order to evaluate the validity of the  $\beta$ -rays derived in Section 2.2.3, we compared them with literature values by Endo, A., et al. (Akira et al., 2005, 2007). The nuclides contributing 1% or more to the decay heat in Table 3,  $^{85}\text{Kr}$ ,  $^{90}\text{Sr}$ ,  $^{90}\text{Y}$ , and  $^{137}\text{Cs}$ , were compared, as shown in Fig. 2 in 0.5 keV steps.

The normalized root-mean-square errors of  $^{85}\text{Kr}$ ,  $^{90}\text{Sr}$ ,  $^{90}\text{Y}$ , and  $^{137}\text{Cs}$  were 2.72%, 2.80%, 1.98%, and 4.08%, respectively.  $^{90}\text{Sr}$ ,  $^{90}\text{Y}$ , and  $^{137}\text{Cs}$  contributed more than 95% of the total decay heat. The  $\beta$ -ray spectra obtained by this method showed good agreement within about 5% between the compared data. These differences are considered to be

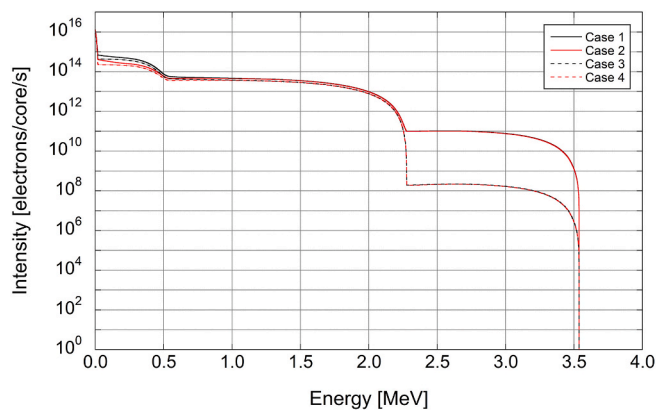


Fig. 2. Comparison of  $\beta$ -rays under the conditions of Case 1, 2, 3, and 4 per core of Unit 2.

mainly due to the differences in the timing of the nuclear data generation. Therefore, it was considered that the method could be appropriately used for simulations.

#### 3.2. Synthesis of the created energy spectrum

Based on the radioactivity data from Section 2.2.1 and the energy spectrum of  $\beta$ -rays determined in Section 2.2.3, synthesized spectra of all the target nuclides were prepared. The results are shown in Fig. 3 in 0.5 keV steps.

There was a remarkable difference in the  $\beta$ -ray intensities of  $^{106}\text{Rh}$  (3.541 MeV) between 11 and 20 years after the accident. In addition, there was a difference in the  $\beta$ -ray intensities below  $\sim 0.5$  MeV between 11 and 20 years after the accident. Furthermore, the average energies of the no FPs release and the release cases after 11 years were 306 keV and 342 keV, respectively, and 330 keV and 378 keV, respectively, after 20 years.

#### 3.3. Comparison of average energies and dose rates of each fuel debris with radii of 0.5, 2.5, and 5.0 cm under the zero FPs release case at 11 years after the accident conditions

In order to determine the conditions under which the effect of bremsstrahlung was the largest, the conditions for the Case 1 were analyzed first, which was when the retrieval of fuel debris samples began. The energy spectra of bremsstrahlung and  $\gamma$ -rays were obtained for fuel debris sizes of 0.5, 2.5, and 5.0 cm and fuel debris compositions of  $\text{UO}_2$ , molten debris, and MCCI products. Fig. 4 shows the energy spectra of the bremsstrahlung,  $\gamma$ -rays, and bremsstrahlung +  $\gamma$ -rays (hereafter, total photons).

As shown in Fig. 4(a), the bremsstrahlung energy spectrum from the MCCI products showed lower intensity than those of the other fuel debris types due to the lower contents of high-Z materials such as actinides, uranium and several FPs. On the other hand, the difference in the energy spectrum intensities of each fuel debris due to size was not as great as the difference in FPs and uranium content due to the volume change. Therefore, it was assumed that the 0.5 cm debris was the most efficient source of bremsstrahlung. The strong peaks between 94 and 112 keV are characteristic X-rays of uranium. In Fig. 4(b), a strong  $\gamma$ -ray peak of 662 keV was emitted from  $^{137\text{m}}\text{Ba}$ , a daughter nuclide of  $^{137}\text{Cs}$ , for each composition and size of the fuel debris. Photons below 662 keV were observed without a sharp decrease because the MCCI products

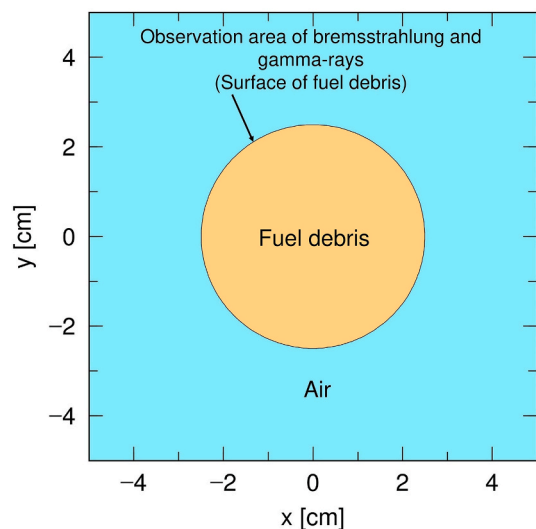


Fig. 3. Schematic diagram of fuel debris and observation area.

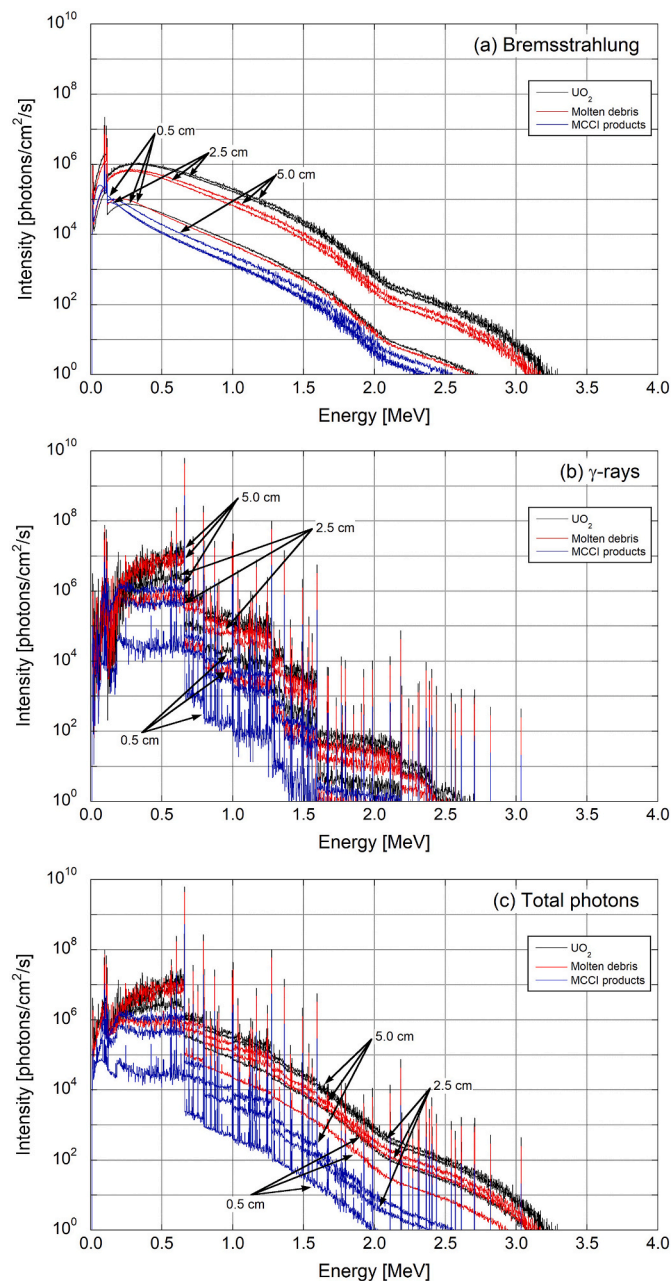


Fig. 4. Energy spectra of (a) bremsstrahlung, (b)  $\gamma$ -rays, and (c) total photons emitted from  $\text{UO}_2$ , molten debris, and MCCI products with radii of 0.5, 2.5, and 5.0 cm under the conditions of Case 1.

were less dense and contained less uranium than the other types of fuel debris. Fig. 4(c) shows that the continuous part of the energy spectrum of total photons was mostly formed by bremsstrahlung. However, the intensity of 662 keV emitted from  $^{137\text{m}}\text{Ba}$  was much higher than that of the continuous part of the bremsstrahlung, and thus a step-like energy spectrum was formed.

Table 5 shows the average energies and dose rates of the bremsstrahlung,  $\gamma$ -rays, and total photons obtained from the energy spectra of Fig. 4.

The effect of bremsstrahlung on the average energy of the total photons was evaluated by the change in the ratio of the average total photon energy to the average  $\gamma$ -ray energy, with a smaller ratio indicating a greater degree of influence of bremsstrahlung. The ratio was the smallest for molten debris with a 0.5 cm radius ( $0.96 \pm 0.15$ ). On the other hand, the fraction of the bremsstrahlung dose rate to the dose rate

of total photons was largest for the  $\text{UO}_2$  with a radius of 0.5 cm ( $3.46\% \pm 0.02\%$ ).

The energy spectrum of the bremsstrahlung was continuously distributed from low to high energy, and the photon intensity was maximum at the low-energy side. The low-energy photons of the generated bremsstrahlung were easily absorbed in the fuel debris, reducing the number of photons of bremsstrahlung on the fuel debris surface. Therefore, for all fuel debris, a radius of 0.5 cm resulted in the highest fraction of bremsstrahlung in the total photon number. In particular, the average bremsstrahlung energy of molten debris, which was high in density and contained a large amount of U with high-Z atomic number, was lower than that of  $\text{UO}_2$ . And because of the large number of photons generated, the ratio of the average energy of total photons to  $\gamma$ -rays was smallest. On the other hand, the fraction of bremsstrahlung in the total dose rate was greatest for  $\text{UO}_2$ , which had the highest average energy and the highest number of photons at 0.5 cm, because the  $H^*(10)$  conversion factor (Akira et al., 2007) used to calculate the dose rate was larger for higher photon energies.

If the radius of the fuel debris is less than the range of the  $\beta$ -rays, the rate of  $\beta$ -ray emissions from the surface of the fuel debris that has not fully emitted any bremsstrahlung will increase. The average  $\beta$ -ray energy under the conditions of the Case 1 was 306 keV, and the range of  $\beta$ -rays based on the continuous slowing down approximation (CSDA) range (ESTAR program; Berger et al., 2017) for  $\text{UO}_2$ , molten debris, and MCCI products in that case were 0.015 cm, 0.024 cm, and 0.042 cm, respectively. Since the maximum energy of the  $\beta$ -rays was higher than the average energy, it is expected that the degree of influence of bremsstrahlung will be greatest at a size somewhat larger than these radii. Therefore, by the time the radius reaches this size, it is estimated that the degree of influence of the bremsstrahlung has already been maximized and has begun to decrease.

#### 3.4. Comparison of average energies and dose rates of $\text{UO}_2$ and molten debris with radius of 0.5 cm under the conditions of zero FPs release and FPs release cases at 11 years after the accident

Here, based on the results obtained in Section 3.1, Cases 1 and 2 were compared in order to evaluate the differences due to the volatile FP release. Fig. 5 shows the combined total photon energy spectrum of the bremsstrahlung and  $\gamma$ -ray results.

The results for all photons in Fig. 5 were similar to those in Fig. 4(c). However, in the FPs release case, the number of photons below 662 keV, the energy of  $\gamma$ -rays emitted from  $^{137\text{m}}\text{Ba}$ , decreased significantly. The continuous part of the photons originating from bremsstrahlung was almost unchanged. Therefore, it was clear that the most significant change in the energy spectrum due to the release of FPs was from the 84% release of Cs.

Table 6 shows the average energies and dose rates of bremsstrahlung,  $\gamma$ -rays, and total photons obtained from the energy spectrum for the FPs release case in Fig. 5.

The ratio of the average energy of all photons to that of  $\gamma$ -rays was the smallest for molten debris, with a value of  $0.85 \pm 0.13$ . The fraction of bremsstrahlung in the total dose rate was higher for  $\text{UO}_2$ , with a value of  $14.90\% \pm 0.06\%$ . Comparing Table 6 with Table 5, these trends were similar for the conditions of both the Case 1 and 2.

The ratios of the photon numbers of bremsstrahlung from the Case 2 to the Case 1 were  $0.93 \pm 0.03$  for  $\text{UO}_2$  and  $0.92 \pm 0.02$  for molten debris. On the other hand, the ratios of the photon numbers of  $\gamma$ -rays from the Case 2 to the Case 1 were  $0.19 \pm 0.03$  for both  $\text{UO}_2$  and molten debris. These results indicate that the main difference between the conditions of the Case 1 and Case 2 was the decrease in the photon number of  $\gamma$ -rays due to Cs release in the Case 2. From the results of subsection 3.3, when comparing the difference between the zero FPs release case and the FPs release case 20 years after the accident, it is clear that the effect of bremsstrahlung has a big impact on the FPs release case than the zero FPs release case. Therefore, in subsection 3.4,

**Table 5**  
Comparison of average photon energies and dose rates under the conditions of Case 1.

Characteristics	Types of fuel debris								
	UO <sub>2</sub>			Molten debris			MCCI products		
Radius (cm)	0.5	2.5	5	0.5	2.5	5	0.5	2.5	5
Average bremsstrahlung energy (keV)	322 ± 5	406 ± 12	423 ± 17	270 ± 4	363 ± 8	390 ± 12	169 ± 3	217 ± 5	239 ± 6
Photon number of bremsstrahlung (photons/cm <sup>2</sup> /s)	2.64E+08	3.87E+08	4.12E+08	1.22E+08	2.14E+08	2.42E+08	4.97E+06	1.56E+07	2.12E+07
Average γ-rays energy (keV)	1.87E+05	5.41E+05	7.48E+05	8.08E+04	2.62E+05	3.60E+05	4.19E+03	1.56E+04	2.56E+04
Photon number of γ-rays (photons/cm <sup>2</sup> /s)	637 ± 18	631 ± 35	633 ± 49	638 ± 15	626 ± 27	621 ± 37	643 ± 12	595 ± 20	567 ± 25
Average total photons energy (keV)	3.82E+09	8.22E+09	9.04E+09	1.69E+09	5.20E+09	6.56E+09	1.08E+08	5.15E+08	9.15E+08
Ratio of the average energy of total photons to γ-rays	±	±	±	±	±	±	±	±	±
Ratio of the photon number of bremsstrahlung to the total photons	2.32E+07	8.36E+07	1.30E+08	9.25E+06	3.92E+07	6.51E+07	5.52E+05	2.75E+06	5.41E+06
Dose rates of bremsstrahlung (Sv/h)	616 ± 16	621 ± 34	624 ± 47	613 ± 14	616 ± 26	613 ± 36	622 ± 11	584 ± 19	560 ± 24
Dose rate of total photons (Sv/h)	0.97 ± 0.17	0.98 ± 0.24	0.99 ± 0.29	0.96 ± 0.15	0.98 ± 0.21	0.99 ± 0.25	0.97 ± 0.13	0.98 ± 0.18	0.99 ± 0.21
Fraction of bremsstrahlung in the total dose rate (%)	0.07 ± 0.02	0.05 ± 0.02	0.04 ± 0.02	0.07 ± 0.02	0.04 ± 0.02	0.04 ± 0.02	0.04 ± 0.01	0.03 ± 0.01	0.02 ± 0.01
	0.02			0.02	0.02	0.02	0.01	0.01	0.01
	1.77 ± 0.00	3.20 ± 0.00	3.54 ± 0.00	0.70 ± 0.00	1.61 ± 0.00	1.94 ± 0.00	0.02 ± 0.00	0.07 ± 0.00	0.11 ± 0.00
	0.00			0.00	0.00	0.00	0.00	0.00	0.00
	51.10 ± 0.30	108.48 ± 1.07	119.68 ± 1.66	22.51 ± 0.12	67.80 ± 0.50	84.77 ± 0.82	1.43 ± 0.01	6.32 ± 0.03	10.71 ± 0.06
	0.30	1.07	1.66	0.12	0.50	0.82	0.01	0.03	0.06
	3.46 ± 0.02	2.95 ± 0.03	2.96 ± 0.04	3.12 ± 0.02	2.37 ± 0.02	2.28 ± 0.02	1.37 ± 0.01	1.16 ± 0.01	1.02 ± 0.01
	0.02			0.02	0.02	0.02	0.01	0.01	0.01

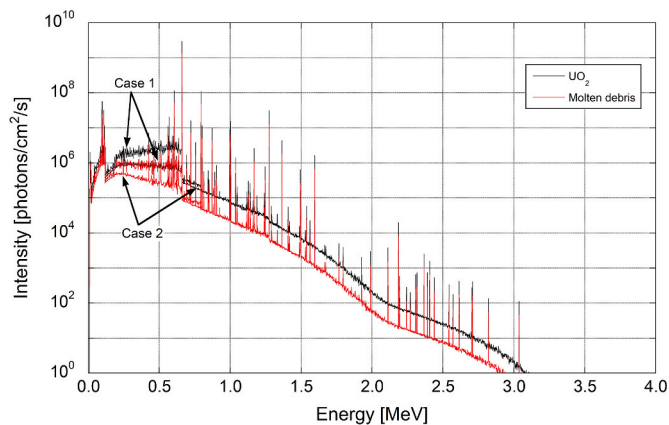


**Fig. 5.** Energy spectra of total photons emitted from UO<sub>2</sub> and Molten debris with a radius of 0.5 cm under the conditions of Case 1 and 2.

**Table 6**  
Comparison of average photon energies and dose rates of UO<sub>2</sub> and Molten debris with a radius of 0.5 cm under the conditions of Case 2.

Characteristics	Types of fuel debris	
	UO <sub>2</sub>	Molten debris
Average bremsstrahlung energy (keV)	331 ± 5	279 ± 4
Photon number of bremsstrahlung (photons/cm <sup>2</sup> /s)	2.45E+08	1.12E+08
Average γ-rays energy (keV)	1.40E+05	5.85E+04
Photon number of γ-rays (photons/cm <sup>2</sup> /s)	667 ± 17	660 ± 14
Average total photons energy (keV)	7.25E+08	3.21E+08
Ratio of the average energy of total photons to γ-rays	±	±
Ratio of the photon number of bremsstrahlung to the total photons	3.72E+06	1.48E+06
Dose rates of bremsstrahlung (Sv/h)	582 ± 12	561 ± 10
Dose rate of total photons (Sv/h)	0.87 ± 0.15	0.85 ± 0.13
Fraction of bremsstrahlung in the total dose rate (%)	0.25 ± 0.03	0.26 ± 0.03
	1.70 ± 0.00	0.67 ± 0.00
	11.38 ± 0.05	4.91 ± 0.02
	0.05	
	14.90 ± 0.06	13.56 ± 0.05
	0.06	0.05

we decided to evaluate only Case 4 and not Case 3.

**3.5. Comparison of average energies and dose rates of UO<sub>2</sub> and molten debris at radius 0.5 cm under the conditions of FPs release cases at 11 and 20 years after the accident**

Based on the results obtained in Section 3.3, the Cases 2 and 4 were compared in order to evaluate the differences due to secular changes. Fig. 6 shows the combined total photon energy spectrum of the bremsstrahlung and γ-ray results.

Fig. 6 shows two major differences between 11 and 20 years after the accident. First, 20 years after the accident, the photon intensity of both the UO<sub>2</sub> and molten debris decreased sharply above ~2 MeV. The second difference was that the total photons decreased in a similar manner for both the UO<sub>2</sub> and molten debris 20 years after the accident.

The reason for the first difference was the decrease of <sup>106</sup>Rh, which has a maximum beta energy of 3541 keV and a half-life of 30.07 s. <sup>106</sup>Rh is a daughter nuclide of <sup>106</sup>Ru with a half-life of 371.8 days. Between 11 and 20 years after the accident, more than 8.8 times the half-life of <sup>106</sup>Ru had passed, and the bremsstrahlung decreased because the amount of <sup>106</sup>Rh decreased. The reason for the second difference was the decrease of <sup>90</sup>Sr, which has a maximum β-ray energy of 546 keV and a half-life of 28.79 years. The daughter nuclide of <sup>90</sup>Sr is <sup>90</sup>Y, which has a maximum β-ray energy of 2280 keV and a half-life of 64.00 h. In particular, <sup>90</sup>Y and

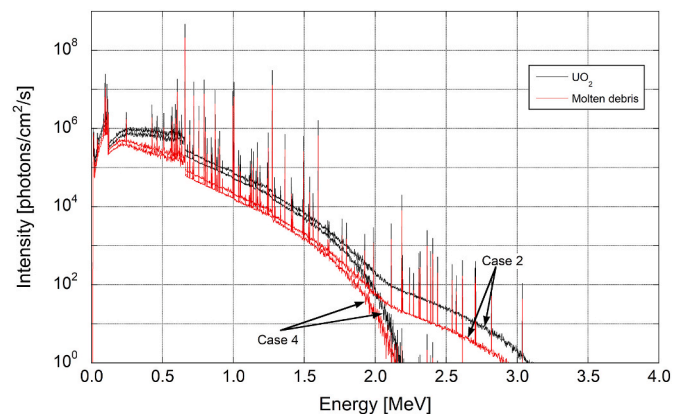


**Fig. 6.** Energy spectra of total photons emitted from UO<sub>2</sub> and Molten debris with a radius of 0.5 cm under the conditions of Case 2 and 4.

**Table 7**

Comparison of average photon energies and dose rates of UO<sub>2</sub> and Molten debris with a radius of 0.5 cm under the conditions of Case 4.

Characteristics	Types of fuel debris	
	UO <sub>2</sub>	Molten debris
Average bremsstrahlung energy (keV)	330 ± 5	278 ± 4
Photon number of bremsstrahlung (photons/cm <sup>2</sup> /s)	1.95E+08 ± 1.11E+05	8.92E+07 ± 4.65E+04
Average $\gamma$ -rays energy (keV)	653 ± 17	650 ± 14
Photon number of $\gamma$ -rays (photons/cm <sup>2</sup> /s)	4.99E+08 ± 3.02E+06	2.20E+08 ± 1.20E+06
Average total photons energy (keV)	563 ± 13	543 ± 11
Ratio of the average energy of total photons to $\gamma$ -rays	0.86 ± 0.15	0.83 ± 0.14
Ratio of the photon number of bremsstrahlung to the total photons	0.28 ± 0.03	0.29 ± 0.03
Dose rates of bremsstrahlung (Sv/h)	1.35 ± 0.00	0.53 ± 0.00
Dose rate of total photons (Sv/h)	7.93 ± 0.04	3.42 ± 0.02
Fraction of bremsstrahlung in the total dose rate (%)	16.97 ± 0.08	15.46 ± 0.07

<sup>90</sup>Sr accounted for more than 95.5% of the decay heat of  $\beta$ -rays 20 years after the accident, and the decrease in these two nuclides caused the overall decrease in the photon intensity of bremsstrahlung.

Table 7 shows the average energies and dose rates of the bremsstrahlung,  $\gamma$ -rays, and total photons obtained from the energy spectra at 20 years after the accident shown in Fig. 6.

Table 7 shows that the ratio of the average energy of all photons to  $\gamma$ -rays was the smallest for the molten debris, with a value of  $0.83 \pm 0.14$ . The fraction of bremsstrahlung in the total dose rate was the highest for UO<sub>2</sub>, with a value of  $16.97\% \pm 0.08\%$ . Therefore, we found that the effect of bremsstrahlung on the average energy and dose rate was greatest under the condition of the Case 4. Comparing Table 7 with Table 6, the average bremsstrahlung and  $\gamma$ -ray energies changed only 1%–2% or less from Case 2 to Case 4. This shows that the decrease in <sup>106</sup>Rh (<sup>106</sup>Ru) had little effect on the average energy and photon number of the bremsstrahlung, although it drastically changed the shape of photon energy spectrum in high energy region. On the other hand, the ratios of the bremsstrahlung photon numbers from the Case 4 to Case 2 were  $0.80 \pm 0.04$  for both UO<sub>2</sub> and molten debris, and those of the  $\gamma$ -rays were  $0.69 \pm 0.06$  for both UO<sub>2</sub> and molten debris. This is mainly attributed to the 19% decrease of <sup>137m</sup>Ba activity, a daughter nuclide of <sup>137</sup>Cs with a half-life of 30.08 years.

#### 4. Conclusion

In order to clarify the conditions under which the effect of bremsstrahlung in the total photons (bremsstrahlung and  $\gamma$ -rays) of fuel debris is maximized, the average energies and dose rates were evaluated from the energy spectra of bremsstrahlung and  $\gamma$ -rays on the fuel debris surface using Monte Carlo simulations. In the simulation, the average energies and dose rates were evaluated with consideration of the composition (UO<sub>2</sub>, Molten debris, and MCCI products), size, volatile FPs release, and retrieval time of the fuel debris.

The ratio of the average energies of the total photons to that of  $\gamma$ -rays was smallest for the molten debris with a radius of 0.5 cm under the condition of the Case 4 (the FPs release case at 20 years after the accident), with a value of  $0.83 \pm 0.14$ , indicating the largest degree of influence of bremsstrahlung. Under the same conditions, the fraction of

bremsstrahlung in the total dose rate was highest for UO<sub>2</sub>, with a value of  $16.97\% \pm 0.08\%$ . Above all, the parameter that had the greatest impact on the total photon mean energy and dose rates was the FPs release case. Unlike conventional spent fuel, fuel debris releases volatile FPs, and the release of <sup>137</sup>Cs, in particular, increases the relative effect of bremsstrahlung on  $\gamma$ -rays. In the case of observing  $\gamma$ -rays emitted from fuel debris, as in the  $\gamma$ -spectrometry, it is easier to observe  $\gamma$ -rays when the fuel debris size is smaller. At the same time, however, it is important to account for the size of the fuel debris because there is expected to be a radius ( $\leq 0.5$  cm) at which the degree of influence of bremsstrahlung is maximized. This work could be expected to contribute to a more realistic evaluation of the influence of average energy and dose rate on matter around fuel debris.

#### Author statement

**Taichi Matsumura:** Conceptualization, Methodology, Formal analysis, Investigation, Writing - Original Draft.

**Keisuke Okumura:** Supervision, Project administration, Writing - Review & Editing.

**Manabu Fujita:** Software, Validation, Data Curation.

**Masahiro Sakamoto:** Resources, Software.

**Kenichi Terashima:** Resources, Investigation.

**Eka Sapta Riyana:** Data Curation, Writing - Review & Editing.

#### Declaration of competing interest

The authors declare that they have no known competing financial interests or personal relationships that could have appeared to influence the work reported in this paper.

#### Acknowledgments

The authors are grateful to Futoshi Minato of JAEA for providing useful technical advice on details of the evaluated nuclear data libraries and their format.

#### References

- Akira, E.N.D.O., et al., 2005. Nuclear Decay Data for Dosimetry Calculation, 38. Revised data of ICRP Publication. JAERI 1347.
- Akira, E.N.D.O., et al., 2007. Nuclear Decay Data for Dosimetry Calculation; Data for Radionuclides with Half-Lives Less than 10 Minutes. JAEA-Data/Code 2007-021.
- Bell, M.J., 1973. ORIGIN: THE ORNL ISOTOPE GENERATION AND DEPLETION CODE. Oak Ridge National Lab.. ORNL-4628.
- Berger, M.J., et al., 2017. Stopping-power & range tables for electrons, protons, and helium ions. NIST Standard Reference Database 124.
- Bottomley, D., Grégoire, A.-C., Carbol, P., Glatz, J.-P., et al., 2006. Fission product and actinide release from the debris bed test Phebus FPT4: synthesis of the post test analyses and of the revaporisation testing of the plenum samples. Nucl. Eng. Technol. 38 (2), 163–174.
- ESTAR program. <https://physics.nist.gov/PhysRefData/Star/Text/ESTAR.html>. (Accessed February 2022).
- Georgeta Radulescu, et al., 2020. Best Practices for Shielding Analyses of Activated Metals and Spent Resins from Reactor Operation. ORNL/SPR-2020/1586.
- ICRP, 1996. Conversion Coefficients for Use in Radiological Protection against External Radiation. ICRP Publication, 74. Ann. ICRP 26 (3-4).
- IRID, 2020. Development of Analysis and Estimation Technologies for Fuel Debris Characterization Results for FY2019.
- Jun-ichi Katakura, et al., 2016. JENDL Decay Data File 2015, JAEA-Data/code 2015-030. JAEA.
- Kai, S.I.E.G.B.A.H.N., 1955. Beta-and Gamma-Ray Spectroscopy. North-Holland Pub, Amsterdam.
- Matsumura, Taichi, et al., 2020. Evaluation of energy spectrum around structural materials in radiation environments. RPC 166, 108493.

- Nishihara, Kenji, et al., 2012. Estimation of Fuel Compositions in Fukushima-Daiichi Nuclear Power Plant, JAEA-Data/Code 2012-018. JAEA.
- Okumura, Keisuke, et al., 2013a. Nuclear data for severe accident analysis and decommissioning of nuclear power plant. In: JAEA-conf 2013-002.
- Okumura, Keisuke, et al., 2013b. Nuclear data for severe accident analysis and decommissioning of nuclear power plant. In: Proc. 2012 Symposium on Nuclear Data. Kyoto University, Japan, JAEA-Conf 2013-002, pp. 15–20.
- Olsen, Charles S., et al., 1988. Examination of Debris from the Lower Head of the TMI-2 Reactor. GEND-INF-084.
- Pusa, Maria, 2011. Rational approximations to the matrix exponential in burnup calculations. Nucl. Sci. Eng. 169, 155–167.
- Sapta Riyana, Eka, et al., 2020. Gamma detector response simulation inside the pedestal of Fukushima Daiichi nuclear power station. MEJ 7 (3).
- Sato, Tatsuhiko, et al., 2018. Features of particle and Heavy ion Transport code System PHITS version 3.02. J. Nucl. Sci. Technol. 55, 684–690.
- Seltzer, Stephan M., et al., 1985. Bremsstrahlung spectra from electron interactions with screened atomic nuclei and orbital electrons. Nucl. Instrum. Methods B12, 95.
- TEPCO, 2021. Mid-and-Long-Term Decommissioning Action Plan 2021.
- Terashima, Kenichi, et al., 2021. A prediction method for the dose rate of fuel debris depending on the constituent elements. J. Adv. Simulat. Sci. Eng. 8 (No. 1), 73–86.
- Tomooki, S.H.I.B.A., et al., 2017. Simple method to create gamma-ray-source spectrum for passive gamma technique. Energy Proc. 131, 250–257.